A modular designed ultra-high-vacuum spin-polarized scanning tunneling microscope with controllable magnetic fields for investigating epitaxial thin films

Kangkang Wang,[a] Wenzhi Lin,[a] Abhijit V. Chinchore, Yinghao Liu,[b] and Arthur R. Smith[c]
Department of Physics and Astronomy, Nanoscale and Quantum Phenomena Institute, Ohio University, Athens, Ohio 45701, USA

(Received 8 March 2011; accepted 12 April 2011; published online 11 May 2011)

A room-temperature ultra-high-vacuum scanning tunneling microscope for *in situ* scanning freshly grown epitaxial films has been developed. The core unit of the microscope, which consists of critical components including scanner and approach motors, is modular designed. This enables easy adaptation of the same microscope units to new growth systems with different sample-transfer geometries. Furthermore the core unit is designed to be fully compatible with cryogenic temperatures and high magnetic field operations. A double-stage spring suspension system with eddy current damping has been implemented to achieve $\leq$5 pm z stability in a noisy environment and in the presence of an interconnected growth chamber. Both tips and samples can be quickly exchanged *in situ*; also a tunable external magnetic field can be introduced using a transferable permanent magnet shuttle. This allows spin-polarized tunneling with magnetically coated tips. The performance of this microscope is demonstrated by atomic-resolution imaging of surface reconstructions on wide band-gap GaN surfaces and spin-resolved experiments on antiferromagnetic $Mn_3N_2(010)$ surfaces. © *2011 American Institute of Physics*. [doi:10.1063/1.3585986]

I. INTRODUCTION

Low-dimensional electronic and magnetic material systems, such as graphene, epitaxial thin films of III-V semiconductors, and transition metal monolayers, have been a subject of intense interest in the past few decades because they often raise intriguing scientific queries and also have great impacts on industrial applications. Nowadays, such materials are normally prepared in ultra-high-vacuum (UHV) chamber systems with advanced growth [such as molecular beam epitaxy (MBE)] capabilities for achieving excellent atomic ordering and cleanness. The scanning tunneling microscope (STM) has proven to be a powerful surface characterization tool since its invention, providing unparalleled information on structural, electronic and magnetic properties (using spin-polarized tips) down to the atomic scale.[1–3] It is often desirable to investigate freshly prepared epitaxial surfaces with STM, either at room-temperature or at cryogenic temperatures. This requires the ability to transfer samples *in situ* from a growth chamber to the STM chamber, which is often realized by an interconnected chamber system employing the use of gate valves to isolate separate chambers.

In practice, different materials often require different growth techniques. This requirement, together with the need for avoiding cross-contamination, results in the need to adapt a variety of sample holders to the STM sample stage. To achieve this, STM's are usually individually designed and constructed to suit the particular application. Whereas, it would be highly desirable to have a modular design that enables easy and quick adaptation of the same essential microscope units to sample holder geometries from different types of growth systems. By constructing multiple replicas of the same modular units, both time and cost can be dramatically reduced.

In our case, we have two UHV systems (A and B) which require STM for surface characterization. System A is a molecular-beam-epitaxy system mainly for the growth of nitride materials with transition metals and transition metal dopants. This MBE chamber is interconnected with an STM chamber which houses a room-temperature STM and other surface-analysis tools such as Auger spectroscopy. System B is a multi-chamber UHV system featuring a larger growth chamber containing both MBE and pulsed laser deposition capabilities and an STM chamber housing a low/variable-temperature STM mounted within a cryostat with a split-coil superconducting magnet. We have developed a modular design of the STM head unit which has been applied to both systems successfully. In this paper, the details of this modular design and its implementation in system A, the room-temperature STM system, will be described, while its implementation in system B, together with full information on the multi-chamber functionalities, will be reported separately.

II. STM DESIGN

A. Core module and the approach mechanism

The core module is designed to be easily transferable between the two chamber systems. This raises several criteria

[a] These two authors contributed equally to this work.
[b] Present address: MPA-CINT, MS K771, Los Alamos National Laboratory, Los Alamos, NM 87545, USA.
[c] Author to whom correspondence should be addressed. Electronic mail: smitha2@ohio.edu.

for the design. The first criteria is that, since the two chamber systems employ different sample holder designs due to different functionalities involved, the STM design has to be able to accommodate both. Considering this and possible future adaptations to other chamber systems, we have decided to leave the sample holder part out of the core module while keeping all the other essential components. This includes the approach mechanism, prism, scanner, and tip holder assembly. For adaptation to a new system, only a sample holder scheme has to be designed and joined to the modular unit. The second criteria is that the design has to work in different orientations (horizontal and vertical). This is due to the fact that different chamber systems employ different sample transfer geometries. This rules out many choices for the approach mechanism, and requires one that works irrelevant of orientation. The third criteria is that the same module should be operational at both room temperature and cryogenic temperatures (~4 K), as well as in high magnetic fields for spin-polarized applications. This poses stringent material requirements such as high thermal conductivity and low magnetic susceptibility.

The finished design of the module unit is shown in Figs. 1(a) and 1(b). As can be seen from these figures, an overall cylindrical shape is chosen because it easily fits into most cryostat bores and also because it is a symmetrical design which can help reduce lateral thermal drifts. The cylindrical body has clearance holes on both of the end plates (item number 6 in Fig. 1(b)), allowing it to be easily joined with other STM components. For the body material, phosphor bronze is selected for its high thermal conductivity, low susceptibility, easiness to machine and relative low cost. This material has been previously successfully implemented in low-temperature and high-magnetic-field STM applications.[4] Other materials have also been used in low-temperature setups, such as MACOR,[5] coin silver,[6] and titanium.[7]

The approach mechanism is based on S. H. Pan's design[8,9] which is proven worldwide to be stably working at different temperatures (down to 10 mK in a recent report by Y. J. Song[6]) and also at different orientations. Our implementation of this design involves a moving prism made of sapphire and six homemade shear-piezo stacks for driving the prism in the so-called stick-slip motion.[5,10] The sapphire prism is polished on all outside surfaces, and the piezo-stacks are capped with high-purity alumina (Al_2O_3) pads for increased wear-resistance during coarse approach cycles. In our application, EBL#4 (from EBL Products Inc.) is selected as the piezo material. Four layers of equal-thickness piezo plates with alternating polarization direction are glued together to form one stack. This configuration increases the total shearing distance by a factor of 4 compared to a single-layer configuration. As can be seen from Fig. 1(b), the six piezo stacks are glued onto three separate bronze beams, with the lower two beams bolted onto the body while the upper beam is pressed by a thin molybdenum leaf spring [item No. 2 in Fig. 1(b)]. The four screws on the leaf spring define the pressure applied to the piezo-prism contact, while a stainless steel ball is placed in between to evenly distribute the pressure. The approach step size can be tuned by varying the applied voltage as well as varying the pressure applied by the leaf spring. For typical applications, a shearing distance of ~120 nm at room temperature and ~50 nm at 77 K are obtained for every 100 V applied across the stack. Different from previous designs where the piezo stacks are glued directly to the body,[4–6,11] here separate beams are used for supporting these stacks which has two advantages: (1) In the case of piezo breakdown, this design enables quick exchange of the piezo actuators without re-machining the body. (2) It allows different sets of stacks with different dimensions to be adapted easily without redesigning the entire body.

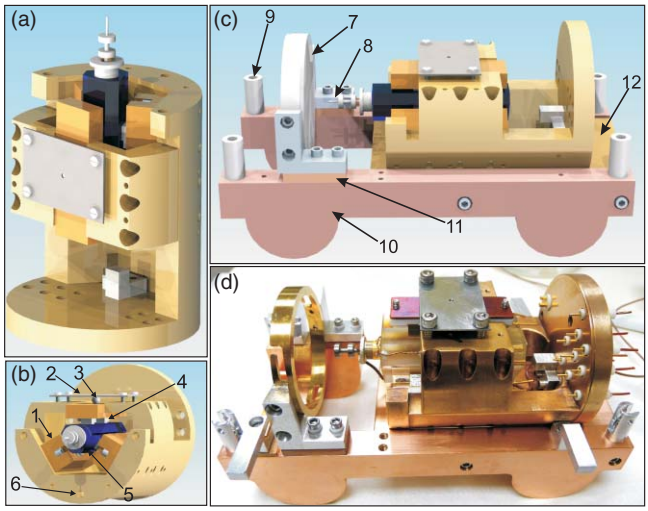

FIG. 1. (Color online) ((a), (b), and (c) are generated using solid edge) (a) side perspective view of the core module; (b) front perspective view of the core module. 1: metal beam where piezo stacks are glued; 2: molybdenum leaf spring; 3: stainless steel ball; 4: piezo stack; 5: sapphire prism; 6: tapped and clearance holes for joining the core module to other components; (c) perspective view of the STM body. 7: sample holder receptacle; 8: tip; 9: posts for spring suspension; 10: oxygen-free high-conductivity copper plates for eddy current damping; 11: MACOR plate for isolating the sample bias voltage; 12: base plate for supporting the core module; (d) real photo of the assembled STM stage.

For scanning, a tube scanner made of EBL#4 piezo material is glued at one end into the center of the sapphire prism via a MACOR bushing. A proper sized scanner has to be chosen such that it provides not only sufficient scan range at low temperatures but also fine enough resolution at room temperature. Here a scanner which is 1 in. in length and 0.02 in. in wall-thickness is selected, which results in ~20 nm/V for x and y and ~5 nm/V for z at room temperature. The scan range is normally reduced by a factor of 2 to 3 when cooling down to 4 K.

B. Adaptation for the room-temperature setup

For our room-temperature setup, the sample surface normal direction always stays horizontal as determined by the sample transfer geometry. This requires the STM core module to be also lying horizontally. To achieve such a configuration, we have designed a rectangular base plate (Item No. 12 in Fig. 1(c)) for supporting the core module. The cylindrical module sits snugly into a matching cut-out in the base plate, then six bolts are inserted (three on the front, as shown in Fig. 1(b) item 6, and three on the back) to firmly join the module to the base plate. The base plate is then bolted to two parallel copper beams (Fig. 1(c) item 10) which have semicircular protrusions for eddy-current damping purposes.

The sample holder ring (Fig. 1(c) item 7) is mounted onto the copper beams via two MACOR plates (Fig. 1(c) item 11) for isolating the sample bias voltage. Four aluminum spring posts (Fig. 1(c) item 9) are then installed onto the end of the two copper beams for suspending the entire support structure with four extension springs. In order to lock down the STM for sample transfer purpose, a pushing-foot travels downward and presses against a crossover bridge (not shown) that is installed over the leaf spring (Fig. 1(b) item 2). After the sample is transferred onto the sample holder ring, the STM support structure can then be released into free suspension state for imaging.

C. Tip exchange and transfer

For *in situ* scanning of epitaxial thin films, a tip exchange mechanism is normally indispensable. This is because of the fact that many epitaxial films do not possess the softness, flatness, and high-conductivity of single-crystal noble metal surfaces (Ag, Au, Cu etc.). While short voltage pulses during tunneling can still be used to modify the tip, exchanging to a freshly prepared tip is often necessary for achieving atomic resolution. For spin-polarized STM imaging where the tip is coated with magnetic materials, the tip exchange mechanism is even more important because a certain fraction of the coated tips may not have the desired magnetic properties.

The tip holder in our setup is machined out of a single piece molybdenum or non-magnetic stainless steel cylinder, as shown in Fig. 2(a). For normal tips made out of W wires (0.02 in. in diameter), the blunt end of the tip is bent by a small angle and forced into the center hole in the tip holder. The bent-created spring force will hold the tip snugly in place. For tips made out of brittle materials such as Cr rods, a set screw is used for holding the tip. The tip holder is then held by a leaf spring in a V-shaped groove, which is glued in a MACOR receptacle mounted on the end of the scanner. For transferring the tip in vacuum, we modified the sample holder design into a tip shuttle which can carry up to 4 tips at once, as shown in Fig. 2(b). For tip exchange, a manipulator with 5 degrees of freedom is used (x, y, z, rotation, and pincher). The cutout on the jaw is shaped to match the center neck of the tip holder, as shown in Fig. 2(c). We intentionally made the cutout to be slightly larger than the neck diameter of the tip holder, which allows the tip to wobble slightly when being held in the jaw. The benefit of this is letting the tip auto-align itself while being inserted into the V-groove, which avoids unwanted stress build-up that can potentially crack the scanner tube. The jaw also has an extra function which is to shift the sample position relative to the holding clips after growth in order to make electrical contact to the freshly grown surface. This step is critical if insulating substrates such as sapphire or MgO are used in the growth.

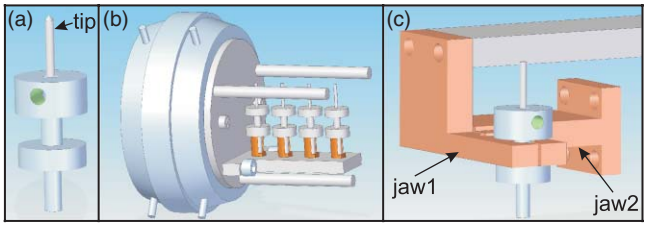

FIG. 2. (Color online) (a) Tip holder with tip; (b) tip holder shuttle with four tip holders; and (c) manipulator jaw grabbing a tip holder.

For normal scanning, W wires are electrochemically etched using NaOH solution and e-beam annealed using an *in situ* setup, in which the jaw acts as an electrical conductor applying a positive high-voltage to the tip. For spin-polarized experiments, the annealed W tips are transferred to the MBE chamber for Fe coating, then transferred back for further mild annealing before being inserted into the STM. A tip garage made out of aluminum is placed in the STM chamber for storing up to 12 tips as well as for magnetizing the tip with a stock permanent magnet. Furthermore, a permanent magnet can be brought into close proximity to the tip-sample junction for applying an external magnetic field of up to 0.4 T, either parallel or perpendicular to the tip axis depending on the magnet configuration, as described in Sec. II E.

D. Vibration isolation system

The exponential dependence of the tunneling current on the tip-sample distance makes vibration isolation extremely critical for achieving atomic resolution. This is especially true for our room temperature setup because the MBE-STM chamber is housed in a room located directly above our mechanical machine shop. Using a seismic accelerometer, the floor vibration is determined to be larger than the vibration criterion standard VC-A (max level 50 μm/s rms (Ref. 12)), much larger than some specially constructed STM lab floors with an isolated foundation which can achieve <VC-E, max level 3 μm/s rms).[6,9] Vibrational peak amplitudes in our MBE-STM lab also have random spikes exceeding 10 μm. Moreover, the interconnected MBE chamber is constantly being pumped by a mechanical pump and a turbo pump which adds additional vibrations to the system. In order to achieve atomic resolution, a stability better than at least 10 pm is required, which demands over 10^6 reduction (or 120 dB) in vibrational amplitude.

In order to achieve the required amount of vibration decoupling, we employ a set of laminar-flow air legs for isolating the chamber system from the floor. The vertical resonant frequency of the air-leg system is <1 Hz. Then a double-stage spring suspension system is implemented to isolate the STM head from the chamber, together with eddy-current dampers using samarium-cobalt magnets. A schematic of the setup is shown in the left side of Fig. 3.

For a single spring damping system, the *transfer function* or the *response function* can be calculated to be[13]

$$K(\omega) \equiv \left|\frac{x_1}{X_0}\right| = \sqrt{\frac{\omega_0^4 + 4\gamma^2\omega^2}{(\omega_0^2 - \omega^2)^2 + 4\gamma^2\omega^2}}, \qquad (1)$$

where x_1 and X_0 are the displacements of the suspended mass and the frame, respectively. $\omega_0 = \sqrt{k/M}$ is the natural

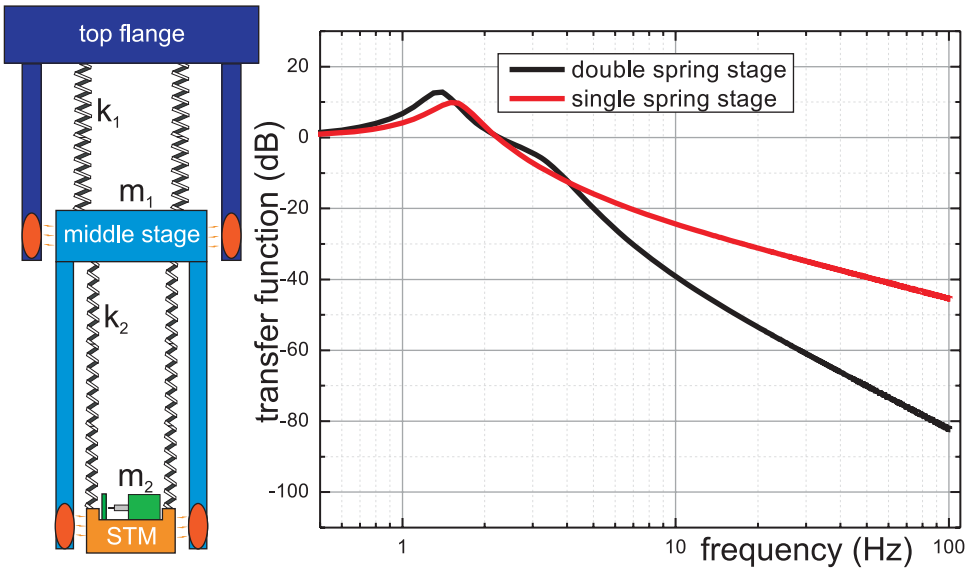

FIG. 3. (Color online) Left: Schematic showing the two-stage spring suspension system with eddy current damping. Right: Calculated vibration transmission response curves. Parameters for our setup are: $k_1 = 0.50(\times 4)$ lb/in. and $k_2 = 0.42(\times 4)$ lb/in. (4 springs per stage); $m_1 = 1.97$ kg and $m_2 = 1.6$ kg; $c_1 = 12$ Ns/m and $c_2 = 8$ Ns/m (total for all magnets acting on that stage).

frequency of the spring system, while $\gamma = c/2M$ is the damping constant. One can propagate such analysis to a two-stage spring system and obtain the combined transfer function[14]

$$K(\omega) \equiv \left|\frac{x_2}{X_0}\right| = \left|\frac{(k_1+ic_1\omega)(k_2+ic_2\omega)}{-k_1[k_2+\omega(ic_2-m_2\omega)]+\omega\{c_1[-ik_2+\omega(c_2+i\omega m_2)]+\omega[k_2(m_1+m_2)+i\omega(c_2(m_1+m_2)+im_1m_2\omega)]\}}\right|, \tag{2}$$

where x_2 is the displacement of the second stage (STM stage); k_1, m_1, and c_1 are the spring constant (per spring), mass, and damping factor (total) for the first stage (middle stage), respectively, and k_2, m_2, and c_2 are the same parameters for the second stage (STM stage). For our setup, the transfer function for the double stage as well as the first stage alone are computed numerically based on these two equations, and the resulting decibel values ($Z = 20\log_{10} K$) are plotted against the driving frequency in the right half of Fig. 3. As can be seen, besides a slight trade-off below 5 Hz, the double-stage spring suspension system is superior to the single-stage configuration. Additionally, Viton rings are wrapped around the end of each spring, providing extra cushioning to prevent high-frequency vibrations from traveling down the spring wires. The overall transfer function from external floor vibrations to the tip-sample gap distance is then a product of all transfer functions, including the transfer function of a rigid STM head assembly, which normally has a very high resonant frequency (several kHz) and a high Q-factor. Combining these vibration isolation mechanisms, we are able to achieve a stability of better than 5 pm, as demonstrated in Sec. III. While this value is larger than some ultrastable STM's constructed specifically for high-energy resolution spectroscopy studies,[6,7,9,15] it is sufficient for most atomic-resolution imaging as well as dI/dV conductance mapping experiments.

E. External magnetic fields

It is often desired to have the capability of applying a tunable magnetic field to the tip-sample junction; this is certainly the case for spin-polarized STM applied to magnetic layers, as well as applications involving the study of superconducting thin films. In the case of SP-STM, applying a magnetic field can result in the magnetic configuration of the tip and/or the sample to be modified accordingly, which will result in a change in the magnetic contrast. This effect can be used both to prove the magnetic origin of the observed contrast, and to study the response of the sample/tip magnetization under applied magnetic fields such as magnetic switching and domain motion.

Commonly these days, external magnetic fields are being introduced using liquid helium cooled superconducting magnets surrounding the STM,[4–6] as is the case for our low-temperature system B. Here, for our room-temperature setup, we have also developed a method of introducing a small magnetic field to the tip-sample junction, as shown in Fig. 4. A permanent magnet is glued onto a modified sample holder and can be transferred into the STM chamber via the loadlock chamber. When the STM is freely suspended by the springs, the magnet can be brought close to (but not touching) the back of the sample, leaving a distance down to only a few millimeters from the sample surface. For an *out-of-plane* field

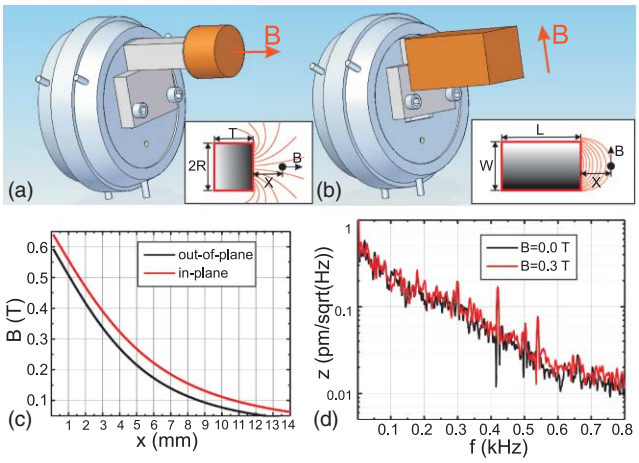

FIG. 4. (Color online) (a) Magnet shuttle carrying a disk magnet for applying *out-of-plane* magnetic fields; (b) magnet shuttle carrying a rectangular magnet for applying *in-plane* magnetic fields. Lower insets illustrate the geometry of the two types of magnets; the gradient gray fill indicates the polarization direction; (c) calculated magnetic fields at distance x (mm) away from magnet surface [at locations of round dots in insets to (a) and (b)]; (d) topographic noise spectra acquired with and without an applied magnetic field, using the same tip, sample, and tunneling condition ($V_s = -0.3$ V, $I_t = 0.2$ nA, preamp gain set at 10^8). The magnet shuttle shown in (a) is placed ~50 mm and ~3 mm away from the sample for these measurements, respectively.

configuration, we chose a disk-shaped magnet which is polarized along its axis (see Fig. 4(a)). For an *in-plane* field, a rectangular magnet polarized through its thickness is used (see Fig. 4(b)).

The strength of the magnetic field at the tip-sample junction can then be controlled by adjusting the magnet-sample distance. For disk magnets, the magnetic field strength at a distance X away from the surface can be estimated by

$$B(X) = \frac{B_r}{2}\left(\frac{T+X}{\sqrt{R^2+(T+X)^2}} - \frac{X}{\sqrt{R^2+X^2}}\right), \quad (3)$$

where B_r is the remnant magnetic field, T is the thickness of the disc magnet, and R is the radius of the disc magnet (as shown in the inset to Fig. 4(a)). For a rectangular magnet, the magnetic field at distance X away from the surface (along the central line) can be estimated by

$$B(X) = \left(\frac{B_r}{\pi}\left(\tan^{-1}\frac{W^2}{2X\sqrt{4X^2+2W^2}} - \tan^{-1}\frac{W^2}{2(L+X)\sqrt{4(L+X)^2+2W^2}}\right)\right), \quad (4)$$

where W is the width of the magnet, and L is the length, as shown in the inset to Fig. 4(b). For our application, we chose neodymium iron boron (NdFeB, N52 standard) magnets for their high remnant magnetic moments (~1.45 T). The magnetic field values for our magnets are computed as a function of the sample-magnet distance X, and plotted in Fig. 4(c). As we can see, a field of up to ~0.2–0.4 T can be achieved at the tip-sample junction. While this field is small compared to fields produced by most superconducting magnet systems (easily several Tesla's or higher[5,6,9]), it is large enough to modify the magnetic configuration of certain magnetically coated tips and sample domain wall structures. For example, a field of ~0.15 T is sufficient to rotate the tip magnetization direction *in-plane* for an Fe-coated W tip.[16]

We also estimated the stray field of the eddy current damping magnets at the tip-sample junction to be <1 mT, which therefore has a negligible contribution to the applied magnetic field. One may think that by bringing a magnet lying on the transporter arm close to the STM head may compromise the vibration damping performance. In our case, since the STM head is made out of non-magnetic materials, the external magnet has negligible effect. The only effect the magnet introduces is an extra term in the damping constant, but this extra term is rather small compared to the overall damping constant. The negligible influence on the vibration isolation is best illustrated in Fig. 4(d) where a pair of topographical noise spectra are taken sequentially with the external magnet far away first, and then brought in ~3 mm away from the sample. The tip is retracted by ~300 nm during shifting of the magnet (to avoid tip crash), and released again when the magnet is in position. By comparing the two spectra, we see that there is essentially no difference; and we can conclude that the magnet has indeed a negligible effect on the vibration isolation performance.

F. Electrical connections

The back end of the core module (opposite to the tip side) is designed to be an electrical contact pad where signal wires coming from the mounting flange are anchored, after which they move on to their target locations. Within the STM head, 0.008 in. thick coated copper wires are used for all signals except the tunneling current signal. For connections from the STM head to the mounting flange, thinner copper wires (0.003 in. outside diameter) are used for reduced vibration coupling. Two sections of coaxial cables are used for carrying the tunneling current, with a short twisted thin copper wire pair for jumping over from the STM stage to the middle stage. To avoid ground loops, a star pattern grounding scheme is implemented, with the STM electronics ground as the center grounding reference point, and with the different stages as terminal points. Furthermore, opposite scanner voltage wires (X+ and X−; Y+ and Y−) are twisted together to reduce their radiating electromagnetic fields. These measures, together with an all-metallic body design, result in a base electronic noise floor below 10 fA, with the highest peak of ~40 fA at 60 Hz (U.S. mains frequency).

III. DEMONSTRATION OF FUNCTIONALITY

A. Atomic resolution

The performance of the completed STM setup is tested on a model epitaxial system – the GaN(000$\bar{1}$) growth surface. Under typical MBE growth conditions, various well-defined surface reconstructions (3×3, 6×6, and c(6×12)(Ref. 17) occur depending on the Ga coverage. Also, the growth fronts follow a spiral growth mode with screw-dislocations at the centers of the spirals.[18] This provides both an ideal testing ground for atomic resolution and an atomic-scale grid for calibrating the scanner (x, y, and z).

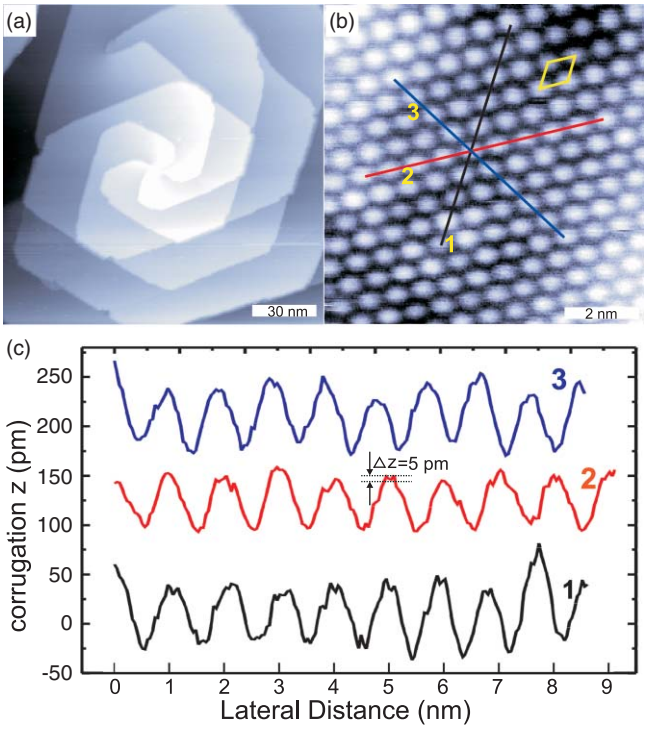

FIG. 5. (Color online) (a) Spiral-mode growth of GaN(000$\bar{1}$) surface. $V_s = 2$ V, $I_t = 0.1$ nA; (b) zoom-in to a 3 × 3 reconstructed area on the GaN surface. $V_s = -0.6$ V, $I_t = 0.1$ nA. The rhombus depicts the 3 × 3 unit cell; (c) stacked topographic height profiles taken along three different lines as labeled in (b).

The growth procedure is the same as reported before by Smith *et al.*[18] Following the growth, the sample is immediately transferred *in situ* to the STM chamber, where it is allowed to cool down to room temperature before scanning starts. Annealed W tips are used in this study. As shown in Fig. 5(a), a growth spiral can be clearly seen forming a flower-like feature. GaN bi-layer steps (~2.6 Å) are observed between each two adjacent terraces. A zoom-in on a 3×3 reconstructed area is shown in Fig. 5(b) where atomic protrusions are clearly visible. To analyze the noise amplitudes, raw images are shown here which have only been background subtracted. Three line profiles are shown in Fig. 5(c), taken along three equivalent directions of $\langle 11\bar{2}0\rangle$. The atomic corrugation amplitude amounts to ~50 pm, whereas the average noise peak-peak amplitudes are measured to be ~5 pm for all three directions. One may note that the unit cell shown in Fig. 5(b) is slightly distorted from an ideal rhombus; this is because of thermal drift caused by temperature variations in the room. A careful examination of the unit cell rhombus reveals a distorted angle of 58° (ideally 60°). Based on our imaging speed (160 nm/s), the size of the rhombus (0.96 nm) and the pixel density (256 pixel/10 nm), the drift velocity is estimated to be ~45 nm/h. Smaller drift velocities (<10 nm/h) are usually observed if imaging is taking place at midnight when the temperature variation in the building is minimal.

B. Spin-polarized experiments

By coating an annealed W tip with ~40 monolayers of Fe, the tip becomes spin-polarized with an *in-plane* magnetization. Here we apply this type of Fe/W tip to a row-wise antiferromagnetic surface of *in situ* grown $Mn_3N_2(010)$. Sample growth is carried out following the recipe reported by Yang *et al.*[19] A film of ~50 nm thickness is grown followed by immediate transferring to the STM chamber. The STM tips are further pulsed several times during tunneling to modify sharpness. A representative image of the surface morphology is shown in Fig. 6(a) where atomically flat terraces are seen. A zoom-in to the boxed region is shown in Fig. 6(b) where row-like structures are resolved with a period of ~6 Å. These rows correspond to the bulk-ordered N-vacancy rows on the $Mn_3N_2(010)$ surface. With a spin-polarized tip, the tunneling current is enhanced for the rows whose spins are aligned parallel to the tip magnetization, and reduced for the rows whose spins are aligned antiparallel to the tip magnetization. As a consequence, a double-period modulation is superimposed onto the regular spin-averaged corrugation, which results in alternating high and low peak amplitudes. As seen in Fig. 6(b), the high peak corrugation averages to ~25 pm, while the spin signal causes a modulation of ~10 pm.

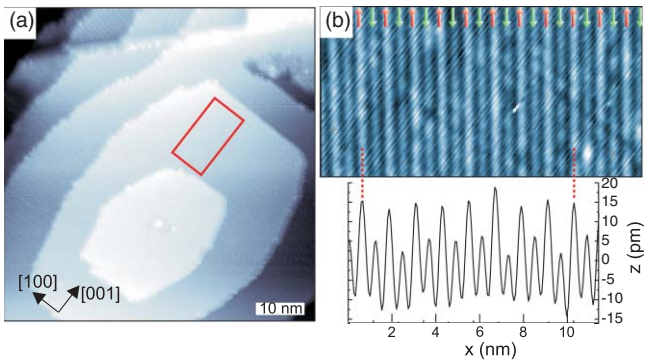

FIG. 6. (Color online) (a) Surface of $Mn_3N_2(010)$ thin film grown on MgO(001) substrate, imaged by an Fe-coated W tip. $V_s = -0.3$ V, $I_t = 0.2$ nA; (b) top: zoom-in to the rectangular area marked in (a); bottom: averaged line profile showing alternating high and low peaks, originating from the row-wise antiferromagnetic spin alignment.

IV. SUMMARY

To summarize, we have developed a modular design for the STM core unit which can be quickly adapted to a variety of UHV systems for operation at various temperatures and in different geometries. The modular unit has been successfully implemented here in a room-temperature setup where a double-stage spring suspension system is employed for achieving high tunneling gap stability. Both tips and samples can be easily exchanged *in situ* with the current design, making this setup ideal for imaging epitaxial thin films grown in an interconnected chamber. Furthermore, a tunable external magnetic field can be applied to the tip-sample junction without sacrificing the vibration isolation performance. The functionality of the STM is demonstrated by atomic resolution on GaN(000$\bar{1}$) surface reconstructions and by spin-polarized measurements on antiferromagnetic $Mn_3N_2(010)$ surfaces.

ACKNOWLEDGMENTS

The authors gratefully acknowledge Prof. Saw-Wai Hla for his helpful suggestions on STM noise reduction and troubleshooting; and Mike Gyamfi and Thomas Eelbo at the University of Hamburg, Germany for insightful discussions on STM design; we also thank Jeremy Dennison and Doug Shafer from the mechanical machine shop for fabricating critical components of the STM. This work is supported by the (U.S.) Department of Energy (DOE), Office of Basic Energy Sciences (Grant No. DE-FG02-06ER46317) and the National Science Foundation (NSF) (Grant No. 0730257).

[1]G. Binnig and H. Rohrer, Rev. Mod. Phys. **59**, 615 (1987).
[2]R. Wiesendanger, *Scanning Probe Microscopy and Spectroscopy: Methods and Applications* (Cambridge University Press, Cambridge, 1994).
[3]R. Wiesendanger, Rev. Mod. Phys. **81**, 1495 (2009).
[4]S. Meckler, M. Gyamfi, O. Pietzsch, and R. Wiesendanger, Rev. Sci. Instrum. **80**, 023708 (2009).
[5]O. Pietzsch, A. Kubetzka, D. Haude, M. Bode, and R. Wiesendanger, Rev. Sci. Instrum. **71**, 424 (2000).
[6]Y. J. Song, A. F. Otte, V. Shvarts, Z. Zhao, Y. Kuk, S. R. Blankenship, A. Band, F. M. Hess, and J. A. Stroscio, Rev. Sci. Instrum. **81**, 121101 (2010).
[7]B. Koslowski, Ch. Dietrich, A. Tschetschetkin, and P. Ziemann, Rev. Sci. Instrum. **77**, 063707 (2006).
[8]S. H. Pan, U.S. patent application WO 93/194,94 (30 September, 1993).
[9]S. H. Pan, E. W. Hudson, and J. C. Davis, Rev. Sci. Instrum. **70**, 1459 (1999).
[10]G. Mariotto, M. D. Angelo, and I. V. Shvets, Rev. Sci. Instrum. **70**, 3651 (1999).
[11]Ch. Witt, U. Mick, M. Bode, and R. Wiesendanger, Rev. Sci. Instrum. **68**, 1455 (1997).
[12]Colin G. Gordon, *Generic Criteria for Vibration-Sensitive Equipment*, Proc. SPIE **1619**, (1991); and *Considerations in Cleanroom Design*, Institute of Environmental Sciences and Technology, RR-CC012.1, (1993).
[13]J. Chen, *Introduction to Scanning Tunneling Microscopy* (Oxford University Press, Oxford, 1993).
[14]M. Okano, K. Kajimura, S. Wakiyama, F. Sakai, W. Mizutani, and M. Ono, J. Vac. Sci. Technol. A **5(6)**, 3313 (1987).
[15]J. H. Ferris, J. G. Kushmerick, J. A. Johnson, M. G. Yoshikawa Youngquist, R. B. Kessinger, H. F. Kingsbury, and P. S. Weiss, Rev. Sci. Instrum. **69**, 2691 (1998).
[16]S. Meckler, N. Mikuszeit, A. PreSSler, E. Y. Vedmedenko, O. Pietzsch, and R. Wiesendanger, Phys. Rev. Lett. **103**, 157201 (2009).
[17]A. R. Smith, R. M. Feenstra, D. W. Greve, J. Neugebauer, and J. E. Northrup, Phys. Rev. Lett. **79**, 3934 (1997).
[18]A. R. Smith, V. Ramachandran, R. M. Feenstra, D. W. Greve, M.-S. Shin, M. Skowronski, and J. Neugebauer, J. Vac. Sci. Technol. A **16**, 1641 (1998).
[19]H. Yang, A. R. Smith, M. Prikhodko, and W. R. L. Lambrecht, Phys. Rev. Lett. **89**, 226101 (2002).